PHYSICAL REVIEW E **77**, 015301(R) (2008)

Bridging kinematics and concentration content in a chaotic micromixer

E. Villermaux,[1,*] A. D. Stroock,[2] and H. A. Stone[3]
[1]*Aix-Marseille Université, IRPHE, 13384 Marseille Cedex 13, France*
[2]*School of Chemical and Biomolecular Engineering, Cornell University, Ithaca, New York 14853, USA*
[3]*SEAS, Harvard University, Cambridge, Massachusetts 02138, USA*
(Received 11 May 2007; published 4 January 2008)

We analyze the mixing properties of the microfluidic herringbone configuration introduced to mix scalar substances in a narrow channel at low Reynolds but large Péclet numbers. Because of the grooves sculpted on the channel floor, substantial transverse motions are superimposed onto the usual longitudinal Poiseuille dispersion along the channel, whose impact on both the mixing rate and mixture content is quantified. We demonstrate the direct link between the flow kinematics and the deformation rate of the mixture's concentration distribution, whose overall shape is also determined.

DOI: 10.1103/PhysRevE.77.015301 PACS number(s): 47.51.+a, 47.61.Ne

Two initially parallel miscible fluid streams flow at an average velocity u along a rectangular channel of small dimensions. By "small," we mean that the width, or height, of the channel's cross section, s_0 (typically 100 μm; see, e.g., [1–3]) is such that the Reynolds number $\mathrm{Re}=us_0/\nu$, where ν denotes the kinematic viscosity, is not large enough for instabilities intrinsic to pipe flows to develop (say, $\mathrm{Re}\lesssim 100$ [4]). Let one of the streams carry a weakly diffusing dye. By "weak," we mean that the Péclet number $\mathrm{Pe}=us_0/D$, where D denotes the molecular diffusivity of the dye, is very large (typically $>10^3$). Initially segregated, the dyed and diluting streams will eventually mix and relax toward a uniform state. If molecular diffusion were solely present, uniformity would require a time $\sim s_0^2/D$. However, the viscous character of the flow and no-slip boundary condition at the channel walls induce internal shears in the fluid that alter significantly the kinetics of the mixing process both at low [5] and large [6,7] Péclet numbers, all the more if in addition the wall has significant topography [8,9]. Similar effects are obtained when the rheology of the fluid is of a viscoelastic type, which mimic a turbulent stirring at viscously dominated scales [2].

The way fluid stirring and molecular diffusion cooperate in hastening the mixing process is readily understood by focusing first on how the flow kinematics increases material contours lengths (see, e.g., [10–13]). In this Rapid Communication, we show how this directly measurable quantity allows us to infer the *mixing time* and the rate at which the mixture's *concentration distribution* $p(c,t)$ subsequently deforms as time t proceeds. An additional feature regarding the randomness of the flow studied here permits us to infer the overall *shape* of $p(c,t)$ as well.

We intend to depict the mixing properties of the staggered herringbone channel, a rectangular channel with grooves on its wall (see Figs. 1 and 2 and [1]). Schematically, the flow is primarily a steady Poiseuille axial flow with transverse rearrangements that produce chaotic trajectories of fluid elements [14]. Consider a blob of volume, say, s_0^3, injected in the channel at time $t=0$. The blob elongates in the direction of the main flow due the transverse shear at a rate $\alpha\sim u/s_0$ so that its streamwise length $L_\parallel$ increases as

$$L_\parallel = s_0(1+\alpha t). \tag{1}$$

The groove-mediated chaotic rearrangements in the channel's cross section result in a sequence of stretch and fold motions realizing a nearly perfect Baker transform (see Fig. 1), which leads to an exponential increase in the length of material lines,

$$L_\perp = s_0 e^{\gamma t}, \tag{2}$$

in the plane perpendicular to the flow direction, clearly seen in Fig. 3 at the early stages of the process when the dye has not started to mix yet. The stretching rate γ is the inverse of the time spent by the mixture through one stirring cycle of the Baker transformation. The blob advected in this tortuous flow pattern thus progressively takes the shape of a convo-

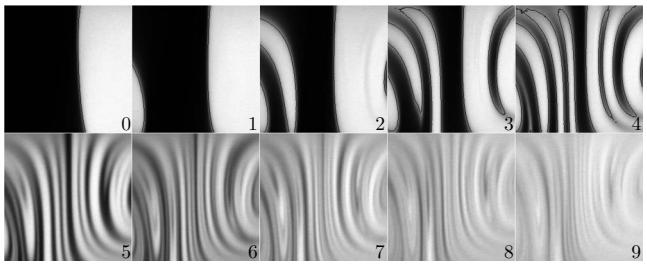

FIG. 1. Scalar field in successive cross sections obtained by confocal microscopy of the staggered herringbone channel of Stroock *et al.* for $\mathrm{Pe}=2\times10^5$, labeled in units m of the stirring cycles (see [1] for the detailed procedure; the images above display the central portion in each section). In the first row labeled from $m=0$ to 4, the field has been stirred, but does not mix yet: the field is essentially composed of concentration $C=0$ and $C=1$ regions, separated by sharp transitions. This allows measurement of the rate of increase of the net material contour length (shown as a dark line tracing the contour with $C=1/2$) as stirring cycles are accumulated. The second row of picture is the subsequent evolution of the mixture above the *mixing cycle* $m_s\simeq 4-5$, and its progressive route toward uniformity.

*Also at Institut Universitaire de France. villermaux@irphe.univ-mrs.fr

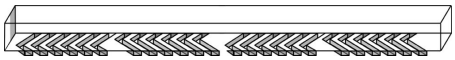

FIG. 2. The staggered herringbone channel [1]. The flow goes from left to right. A stirring cycle is composed of two sequential regions of ridges.

luted sheet whose transverse thickness $s(t)$, such that the volume $s(t)L_{\parallel}L_{\perp}=s_0^3$ is conserved, decays as

$$s(t) = \frac{s_0}{(1+\alpha t)e^{\gamma t}} \underset{\gamma t \gg 1}{\rightarrow} s_0 e^{-\gamma t}. \tag{3}$$

The blob expands linearly in time in the flow direction, but the main contribution to its net area increase comes from the radial multiplicative foldings in the cross-sectional plane.

The scalar field at the entrance of the channel is bimodal, with concentration $C=0$ and $C=1$ injected in streams of equal flow rate, so that the cross-sectionally averaged concentration remains equal to $\langle C\rangle=1/2$ all along the channel. We will therefore count concentrations from the mean, defining $c=2C-1$. Obviously, $\langle c\rangle=0$. The concentration profile of an elementary stretched sheet is governed by

$$\partial_t c + \boldsymbol{u}\cdot\boldsymbol{\nabla} c = D\boldsymbol{\nabla}^2 c, \tag{4}$$

which simplifies if written in a frame $\{x,y\}$ in the channel's cross-section plane whose axes are aligned with the directions of maximal stretching and compression of the sheet—i.e., $\mathbf{u}=(-\sigma x,\sigma y)$ with $\sigma=-d\ln[s(t)]/dt$. Thus Eq. (4) becomes

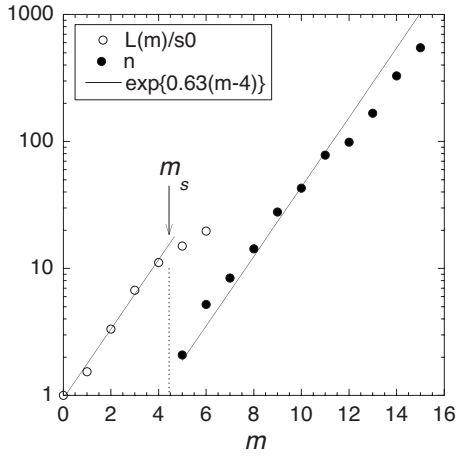

FIG. 3. ○: Material contours length $L_{\perp}(t)/s_0$ measured in the channels' cross section as shown in Fig. 1 before the mixing cycle, when the mixture is still bimodal (i.e., $c=\pm 1$). The increase is fairly exponential and gives, comparing to Eq. (2), an equivalence time-stirring cycles as $\gamma t=0.63m$, close to that which would be expected from a Baker transform where the length doubles at each cycle $(L_{\perp}(m)/s_0=2^m)$. ●: Index n fitted from the concentration distributions in Fig. 4 at each stirring cycle for $m>m_s\simeq 4.5$. Both $L_{\perp}$ and n follow the same rate of increase with m.

$$\partial_t c - \sigma x \partial_x c = D\partial_x^2 c, \tag{5}$$

which expresses that concentration gradients are essentially zero along the lamellar structures formed by the stretch (see Fig. 1) and concentrate across the lamellae in the direction x aligned with the principal axis of the blob compression [11]. This equation, where substrate stirring appears through the apparent stretching rate σ only, is solved in closed form [10,15] and it follows that from the *mixing time*

$$t_{\mathrm{mix}} = \frac{1}{2\gamma\left(1+\frac{\alpha}{\gamma}\right)}\ln\left(2\frac{\gamma s_0^2}{D}\right) \tag{6}$$

the maximal concentration $c_{\max}$ in the sheet starts to decay as

$$c_{\max} = e^{-\gamma(t-t_{\mathrm{mix}})}, \tag{7}$$

while the thickness of the scalar gradient remains constant at $\sqrt{D/\gamma}$ (the Batchelor scale [16]). Beyond the mixing time, the concentration profile $c(x,t)$ across a stretched sheet is, therefore,

$$c(x,t) = \frac{e^{-\gamma(t-t_{\mathrm{mix}})}}{2\sqrt{\pi D/\gamma}} e^{-x^2/(2D/\gamma)}, \tag{8}$$

with an essential invariance in the y direction.

The above result holds as soon as the substrate deformation time γ^{-1} is shorter than the diffusion time s_0^2/D—that is, for $\mathrm{Pe}\equiv\gamma s_0^2/D>1$. In units m of the stirring cycles in the staggered herringbone channel, Fig. 3 shows that the equivalence *time-stirring cycles* is $\gamma t=0.63m$. The number of units it takes for the stirred mixture to start to mix (equivalently the mixing distance) is thus expected according to Eq. (6) to vary like $\ln(\mathrm{Pe})$, as noted in [1], and is also found for a different stirring protocol using droplets in curved channels [17]. With $\mathrm{Pe}=2\times 10^5$ as for the experiment analyzed here, one anticipates from Eq. (6) with $\alpha/\gamma=O(1)$ that $m_s\simeq 4.5$, in close agreement with the observed transitional value between a bimodal field, and a field in the process of being mixed (see also Fig. 4). This suggests in particular that the fields we analyze are not dominated by slow motions near the walls or recirculating regions with closed streamlines, as it might be in other instances [18–20].

Note nevertheless that if the stretching of material lines were to be subexponential leading to, e.g.,

$$s(t) = s_0(1+\gamma t)^{-\beta}, \tag{9}$$

with β some positive number as for flows dominated by persistent shear, then the mixing time would be [15]

$$\gamma t_{\mathrm{mix}} \sim \mathrm{Pe}^{1/(1+2\beta)}, \tag{10}$$

giving thus a power law dependence of the equivalent mixing distance on Pe, as observed with another stirring protocol in a similar context for which, however, the kinematics of the flow was not documented [3].

Sheets are not isolated in the channel and, because of the confinement by the walls, unavoidably overlap and merge. The phenomenon, obvious in Fig. 1, is precisely the one responsible for the ultimate spatial homogeneity of the mixture and is a common feature of mixtures evolving in a con-

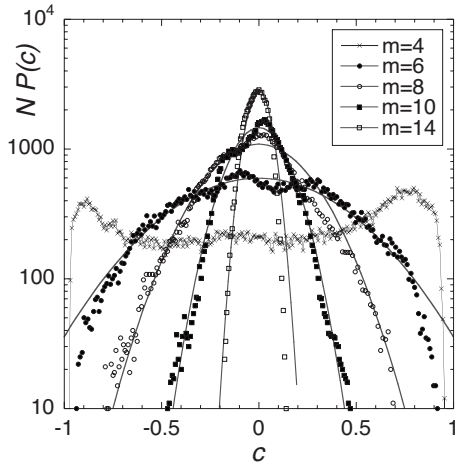

FIG. 4. Concentration distributions $p(c,t)$ measured on two-dimensional cross sections of the flow at successive downstream locations in the channel, as shown in Fig. 1. $N=250^2$ is the number of sampled pixels in each image. The successive sections are labeled in units of the stirring cycles m. For $m<m_s\simeq 4-5$, the scalar field is still bimodal, while for $m>m_s$, it mixes and its concentration content is well represented by Eq. (18). The best fit (solid line) is obtained by adjusting n, whose value for each m location is reported in Fig. 3.

fined environment [15,21]. We next calculate the overall concentration distribution $p(c,t)$ of the mixture. We will, in fact, devise an evolution equation for the maximal concentration $c\equiv c(0,t)$ by neglecting the contribution of the tails of the spatial profile $c(x,t)$ in Eq. (8), an assumption essentially valid for interacting stretched sheets [13]. The distribution is affected by two ingredients, the first being the decay of the concentration levels according to Eq. (7) which, on ensemble average, is written

$$\left\langle \frac{\delta c}{\delta t} \right\rangle = -\gamma c \quad \text{and} \quad \langle c \rangle = \int cp(c)dc = 0. \tag{11}$$

The second ingredient reflects the interaction between the sheets themselves. Owing to the linearity of the convection-diffusion equation (4), that interaction is additive in concentration space. If moreover the addition of the concentration levels in the mixture is made *at random*, then the corresponding evolution rule for $p(c,t)$ is of a *self-convolution* type [15,22,23]. This *maximal randomness* ideal limit is supported by the Poincaré sections of the present flow made in [14] showing that a set of material particles initially localized in small nearby puffs do explore the entire cross section of the channel in an intermingled fashion. An element of a stretched sheet with a given concentration c_1 is thus liable to merge with another one with concentration c_2 with a probability $p(c_1,t)p(c_2,t)$, with no correlation between the sheet's Lagrangian history and the rate of encounter with their neighbor, to give rise, an instant of time later after merging, to a concentration level c with probability $p(c,t+\delta t)=\int p(c_1,t)p(c_2,t)dc_2$ provided $c=c_1+c_2$. The continuous version of this evolution for $p(c,t)$ incorporating both ingredients is written in its most general form as

$$\partial_t p = \gamma \partial_c (cp) + \dot{n}(-p + p^{\otimes 1+1/n}), \tag{12}$$

where $\otimes$ stands for the convolution operator. The (null) average concentration is conserved by Eq. (12) provided $\gamma n = \dot{n}$ which defines, with γ constant, $n(t)$ as

$$n(t) = e^{\gamma t}. \tag{13}$$

A natural choice to look for a similarity solution for $p(c,t)$ is to count concentrations in units of the field standard deviation $\sigma=\sqrt{\langle c^2\rangle-\langle c\rangle^2}$, with $\langle c^2\rangle=\int c^2 p(c,t)dc$. Since $p(c,t=0)=\frac{1}{2}[\delta(c-1)+\delta(c+1)]$ is the initial condition, one has from Eqs. (12) and (13)

$$\sigma^2 = \frac{1}{n}. \tag{14}$$

If time is further counted in units of $n/\dot{n}$, one thus looks for a similarity solution of the form [24]

$$p(c,t) = \frac{1}{\sigma} f(\eta,\tau), \quad \eta = \frac{c}{\sigma}, \quad \tau = \ln(n). \tag{15}$$

Taking the Fourier transform of Eq. (12) with $\tilde{p}(k,t)=\int e^{ikc}p(c,t)dc$, one arrives at

$$k\frac{\partial \tilde{f}}{\partial k} = 2n(-\tilde{f} + \tilde{f}^{1+1/n}). \tag{16}$$

The solution of Eq. (16) is

$$\tilde{f}(k,\tau) = \left(1 + \frac{(k\sigma)^2}{2n}\right)^{-n}, \tag{17}$$

whose inverse in concentration space, with $\sigma=1/\sqrt{n}$, gives finally

$$p(c,n) = \frac{2^{3/4-n/2} n (cn)^{(-1+2n)/2} K_{1/2-n}[\sqrt{2}nc\ \mathrm{sgn}(c)]}{\sqrt{\pi}\Gamma(n)}, \tag{18}$$

where $K_{1/2-n}$ is the modified Bessel function of the third kind of order $\frac{1}{2}-n$ and sgn denotes the *sign* function. This distribution has large excursion exponential tails [25] characteristic of aggregation phenomena [3,15,23],

$$p(|c| \gg 1/\sqrt{n}, n) \sim \exp(-\sqrt{2}n|c|), \tag{19}$$

while its core approximates to a Gaussian of variance σ^2:

$$p(|c| \ll 1/\sqrt{n}, n) \sim \sqrt{\frac{n}{2\pi}} e^{-nc^2/2}. \tag{20}$$

It is seen from Fig. 4 that Eq. (18) is not only a good fit of the overall concentration distribution shape for successive downstream locations in the channel (the bumps of the experimental distributions around the ideal ones are due to a lack of statistical convergence inherent to the limited size of the images), but that its rate of deformation, parametrized by $n(t)$ solely, closely follows the one anticipated from the rate of increase of material lines in the flow [see Eqs. (2) and (13)], with no additional adjustable parameter. This demonstrates the intimate link between flow kinematics and mixing state of the system. Each concentration level in the mixture at a given instant of time results from the merging of n

elementary sheets whose individual concentration decays as $1/n$ [see Eqs. (7) and (13)]. The chaotic motions in the channel ensure that these additions are made at random, generating distributions $p(c,n)$ belonging to the family stable by self-convolution given in Eq. (18). These distributions both feature exponential tails frequently encountered in random advection and a relaxation through a central limit route leading to Gaussians in the well-mixed limit.

[1] A. D. Stroock, S. K. Dertinger, A. Adjari, I. Mezic, H. A. Stone, and G. M. Whitesides, Science **295**, 647 (2002).
[2] A. Groisman and V. Steinberg, Nature (London) **410**, 905 (2001).
[3] C. Simonnet and A. Groisman, Phys. Rev. Lett. **94**, 134501 (2005).
[4] H. Schlichting, *Boundary Layer Theory* (McGraw-Hill, New York, 1987).
[5] G. I. Taylor, Proc. R. Soc. London, Ser. A **225**, 473 (1954).
[6] H. K. Moffatt, Rep. Prog. Phys. **46**, 621 (1983).
[7] L. Biferale, A. Crisanti, M. Vergassola, and A. Vulpiani, Phys. Fluids **7**, 2725 (1995).
[8] H. A. Stone, A. D. Stroock, and A. Adjari, Annu. Rev. Fluid Mech. **36**, 381 (2004).
[9] T. M. Squires and S. R. Quake, Rev. Mod. Phys. **77**, 977 (2005).
[10] W. E. Ranz, AIChE J. **25**, 41 (1979).
[11] P. B. Rhines and W. R. Young, J. Fluid Mech. **133**, 133 (1983).
[12] E. Villermaux and H. Rehab, J. Fluid Mech. **425**, 161 (2000).
[13] P. Meunier and E. Villermaux, J. Fluid Mech. **476**, 213 (2003).
[14] A. D. Stroock and G. M. McGraw, Proc. R. Soc. London, Ser. A **362**, 971 (2004).
[15] E. Villermaux and J. Duplat, Phys. Rev. Lett. **91**, 184501 (2003).
[16] G. K. Batchelor, J. Fluid Mech. **5**, 113 (1959).
[17] H. Song, M. R. Bringer, J. D. Tice, C. J. Gerdts, and R. F. Ismagilov, Appl. Phys. Lett. **83**, 4664 (2003).
[18] Y. Pomeau, C. R. Acad. Sci., Ser. II: Mec., Phys., Chim., Sci. Terre Univers **301**, 1323 (1985).
[19] B. I. Shraiman, Phys. Rev. A **36**, 261 (1987).
[20] M. Chertkov and V. Lebedev, Phys. Rev. Lett. **90**, 034501 (2003).
[21] E. Villermaux and J. Duplat, Phys. Rev. Lett. **97**, 144506 (2006).
[22] R. L. Curl, AIChE J. **9**, 175 (1963).
[23] A. Pumir, B. I. Shraiman, and E. D. Siggia, Phys. Rev. Lett. **66**, 2984 (1991).
[24] S. K. Friedlander and C. S. Wang, J. Colloid Interface Sci. **22**, 126 (1966).
[25] G. N. Watson, *A Treatise on the Theory of Bessel Functions* (Cambridge University Press, Cambridge, England, 1958).